Ceramic Synthetic Substrates Using Solid Freeform Fabrication

William J. Chappell, Chris Reilly, John Halloran, and Linda P. B. Katehi, *Fellow, IEEE*

***Abstract*—Three-dimensional (3-D) printing techniques were used to create lost molds for advanced inhomogeneous materials made of ceramics. The utility of this process is the ability to manipulate low-loss materials, such as alumina illustrated here, into precise, fine features as periodic macroscopic inclusions in a larger host material or air. Three periodic structures were formed using solid freeform (SFF) fabrication techniques; a two-dimensional (2-D) all-dielectric electromagnetic bandgap (EBG) substrate, a 2-D metallo-dielectric substrate filter, and a 3-D woodpile EBG structure. The design of these structures is discussed and the fabricational steps are presented in detail. This process has been utilized to develop a simple two-pole filter embedded in a substrate at 10 GHz, a single resonator at 30 GHz, and a 3-D bandgap structure from 88 to 115 GHz. The wide range of features and structures that can be accurately fabricated are highlighted.**

***Index Terms*—Alumina, bandpass filters, ceramics, dielectric resonators, electromagnetic bandgaps (EBGs), freeform fabrication, high-frequency resonators, high-Q planar filters, metallodielectric lattices, photonic bandgaps, woodpile structures.**

I. Introduction

THE ability to design and fabricate composite and inhomogeneous structures to create artificial dielectrics has been a research focus for many years. The development of inhomogeneous materials gives rise to new material properties that homogeneous materials found in nature do not posses. Synthetic substrates have been developed to alter the dielectric constants of naturally occurring materials as well as manipulate waves by altering the phase of propagation through multiple reflections [1]. Composite or small-scale inhomogeneous materials have the benefit to provide unique intrinsic properties of the material, i.e., thermal expansion and dissipation coefficients, and/or unique propagation characteristics.

Periodic structures, one of the most interesting forms of inhomogeneous materials, have been the focus of much research for the past century [2]. The research has widely increased in intensity the past fifteen years with the interest in electromagnetic (EM)/photonic bandgap structures [3]. It has been found that the correct spacings for periodic inclusions can block energy propagation in multiple dimensions. Therefore, incident energy will evanesce into the material. Equivalently, fields from a source embedded in the material will evanesce as well and be localized. For years, many different applications have been envisioned, including spatial filters, low-loss reflectors, high-quality resonators, waveguides, and highly efficient antenna structures. Implicit in many of these applications is the use of low-loss materials to create the necessary reflection without the dissipation of energy. Therefore, to fully exploit the utility of periodic substrates and to enhance the benefit of this architecture relative to other structures, precise manufacturing of low-loss material is needed.

A barrier to realizing low-loss periodic structures is that many low-loss substrates are difficult to machine or manipulate. There are relatively few methods to manipulate low-loss, high-frequency materials. For example, the highly ubiquitous ceramic, alumina, is an extremely hard substance that cannot be milled, drilled, or etched without great difficulty. This has restricted the fabrication of these materials from very complex shapes like multidimensional periodic structures. To this end we apply the indirect solid freeform fabrication (ISFF) method to high-purity alumina. ISFF of ceramics was recently developed for such varied applications as bone scaffoldings [4], sonar hydrophones [5], and miniature turbines [6]. In short, the ISFF technique refers to the use of suspension polymerization casting of alumina into a lost mold built by a layered manufacturing tool [7], [8].

In this paper, we use the SFF techniques to produce low-loss periodic ceramic structures. Using the layer-by-layer techniques, three different low-loss, precisely aligned periodic structures have been developed. To highlight the abilities of this technique, this process was utilized to develop a simple two-pole filter at 10 GHz, a single all-dielectric electromagnetic bandgap (EBG) resonator at 30 GHz, and a three-dimensional (3-D) "woodpile" bandgap structure from 88 GHz through 115 GHz. The purpose of the three different designs is to both show the unique characteristics of periodic structures and to demonstrate the capabilities of this new fabrication technique. Specifically the three designs illustrate the unique process' loss characteristics, high-frequency application, and precise feature alignment.

The new fabrication techniques are an improvement on three fronts. First, the miniaturization of these structures brings the periodic structures to the realm of practical products, beyond just the proof of concept stages of earlier work. Additionally, the formation of advanced structures into one piece in a single fabrication step without bonding, manual placement or alignment allows repeatable products beyond what could be achieved by amalgamated processes. Third, the loss of the ceramic material is much better than that of previously realized periodic structures.

Manuscript received November 26, 2001; revised July 13, 2002. This work was supported by the Office of Naval Research under Contract RN N00014-01-1-0779 and by the Defense Advanced Research Projects Agency under the Metamaterials Project RN N00 173-01-1-6910.

W. J. Chappell and L. P. B. Katehi are with the Radiation Laboratory, Department of Electrical Engineering and Computer Science, Purdue University, West Lafayette, IN 47907-2035 USA.

C. Reilly and J. Halloran are with the Material Science Department, The University of Michigan at Ann Arbor, Ann Arbor MI 48109-2122 USA.

Digital Object Identifier 10.1109/TMTT.2003.808727

II. Periodic Structures Overview

As stated in the introduction, periodic structures have unique characteristics associated with them. These include the ability to manipulate the dielectric parameters of a material, create slow or fast waves within the material, and of recent interest block energy from propagating for multiple spatial dimensions. This latter property is the focus of this study. Periodic structures have the capability to localize energy by forbidding the propagation of energy over a frequency band. This property can be utilized to develop high-frequency components such as antennas, resonators, and filters [9], [10]. These types of periodic materials have been more recently termed EM or photonic bandgaps. These structures will be referred to as EBGs in an effort to accurately describe the phenomenon and to be consistent with past literature. In the past, two-dimensional (2-D) and 3-D structures have been designed and fabricated but with limiting fabrication issues.

A. 2-D EBG Structures

To explore the application of 2-D periodic structures, the present authors have presented designs for multipole filters utilizing the periodic EBG structures [11] as well as high-Q planar resonators [10]. In short, the lowest order mode of a parallel plate with periodic inclusions is used to block energy from propagating in the substrate. The energy in the substrate is then manipulated using defects in the periodicity to create the desired function, in these cases either resonance or filtering. The original designs were verified by machining of Rogers Corporation's Duroid into the necessary periodic shapes. However, the crude milling procedure limited the ability to design and fabricate the structures for operation at high frequencies. Though useful for the analysis and proof of concept of the structure, the unloaded Q of the resonance was limited by the relatively high loss tangent of the Duroid (loss $\tan \sim 0.003$ and loss $\tan \sim 0.0009$ for the high dielectric material and low dielectric material, respectively). It is the aim of this portion of the research to improve upon the original designs by making the structures smaller and more effective out of low-loss ceramics.

B. 3-D EBG Structures

In an effort to create a 3-D EBG structures, there has been much work previously on the woodpile structures, for example, [12] and [13]. The woodpile structure is comprised of criss-crossed logs that block energy propagation in three dimensions. The initial proof of concept was designed for X-band frequencies. The results showed that the woodpile was a simple way of developing a 3-D EBG substrate. However, the resulting structure is quite large and therefore not practical for many applications. In contrast, smaller, higher-frequency woodpiles have been created but out of micromachined silicon or polysilicon. The resulting polysilicon layers, though minute and precisely defined, would have material losses order of magnitudes greater than that of alumina [13]. It is the aim of this portion of our study to show the fabrication of high-frequency woodpiles in a low-loss ceramic.

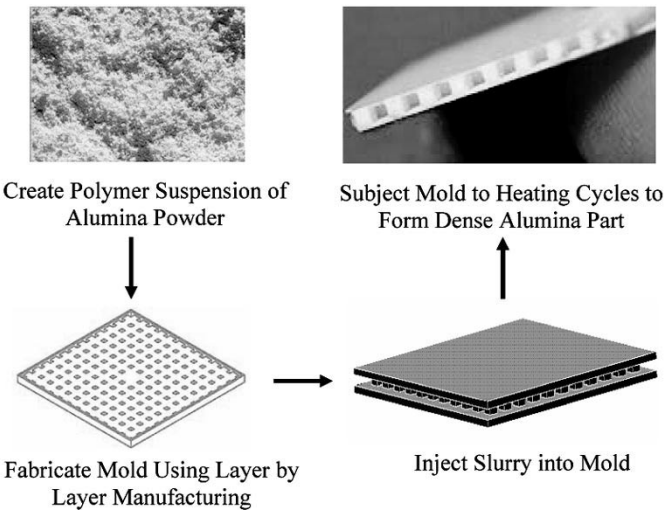

Fig. 1. Basic process for realization of a periodic structure made through ISFF.

III. ISFF Processing Applied to Periodic Dielectrics

A brief overview of the ISFF process is shown in Fig. 1. The part to be built is first created as a solid body in AutoCAD. Next a modified Boolean negative of the part is translated to .stl format so it can be built on the 3-D inkjet printer, a Solidscape Modelmaker Pro II. Layer by layer, the 3-D inkjet printer drops bits of wax for the support or mold regions. This printed structure is then used as a lost mold in the casting process. The slurry that is cast and cured into the lost mold is a 54 vol% alumina dispersed in an acrylate monomer solution. Once the slurry is cured in the mold to form the green part, it is put through one slow heating cycle to thermally remove the mold and binder, and a second cycle to sinter the ceramic into a fully dense alumina part. The geometry of the original computer-aided design (CAD) design is thus replicated in ceramic.

To be more specific, the monomer solution component of the Al_2O_3 (alumina) slurry is a 7:1 mix of isobornyl acrylate monomer (IBA, Sartomer 506, Aldrich, Milwaukee, WI) to propoxylated neopentyl glycol diacrylate monomer (PNGPDA, Sartomer 9003, Aldrich, Milwaukee, WI) which is diluted by 20 vol% with decahydronapthalene (Decalin, Avacado Corporation). The monomer solution is filled with 54 vol% alumina powder, (A-16SG, Alcoa, Pittsburgh PA) powder dispersed with an ammonium acetate-based surfactant. The monomer solution containing the dispersed alumina (referred to as slurry) is cured in the mold via the addition of benzoyl peroxide (BPO, Aldrich, Milwaukee, WI) as an initiator and N,N,Dimethyl-p-toluidine, (NNDPT, Aldrich, Milwaukee, WI) as a catalyst. The solution is initially cooled. Upon heating, the benzyl peroxide decomposes to create free radicals, which initiates the free radical polymerization reaction that converts the liquid acrylate monomer into a solid binder. The curing of the monomer solution creates a polymer network with entrapped ceramic particles in the shape defined by the mold. The catalyst is used to allow the polymerization to occur at room temperature. The polymer binder and mold are both removed by slowly heating the cured part in air to 600 °C. The binder free part consists of a structure that is 54 vol%

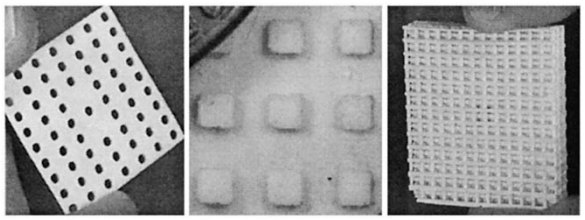

(a) (b) (c)

Fig. 2. Realizations of the three periodic structures made from the ISFF process. (a) Multipole metallodielectric filter. (b) 2-D all-dielectric EBG substrate (cutaway view). (c) 3-D woodpile structure.

alumina and 46 vol% air in the shape defined by the mold. This particle compact is heated to 1650 °C for 2 h to sinter the ceramic into a solid alumina body that is 98.3% theoretical density. The end result is a dense ceramic part in the shape of the original CAD file. However, the volumetric shrinkage intrinsic to the densification is inherently locally nonuniform and results in less than 2% variance in fidelity from the original CAD designed part. This is typical of ceramic parts fabricated from loosely packed powder bodies.

The size scale of the part determines its frequency range of operation. Smaller spacing of the periodic inclusions create interference phenomenon for smaller wavelength/higher frequency EM radiation. The mold-making tool limits the feature size resolution of the final part. When applied to periodic dielectric structures, this means that the feature size resolution of the mold-making tool determines the upper limit of operational frequency range for the structure. The 3-D inkjet printer can safely create structural features on the order of 300 μm in the transverse dimensions with layers of 50.8 μm in the stacking direction. The resolution is limited by the amount of material that the ink jet head drops at each pixel. The structures of interest in this work are designed for communication systems that operate in the X- through W-bands. The molds for these structures are well within our range of manufacturing capability.

The three separate parts formed using this method each demonstrate a particular beneficial feature of this fabrication technique (Fig. 2). The metallodielectric filter demonstrates the low loss of the materials after processing. The 2-D all dielectric resonator shows the application to advanced higher frequency planar structures and the 3-D woodpile demonstrates the application to relatively minute, yet precise 3-D structures operating even higher in frequency. The design and results of these structures are shown below.

IV. Metallodielectric Filter

A metallodielectric periodic structure refers to the formation of a substrate that will not propagate energy because of metallic inclusions periodically embedded in a substrate. The structure consists of a dielectric substrate with ground planes top and bottom, with an array of metal-post inclusions forming via holes connecting the ground planes. These inclusions are less than a half wavelength apart in the bandgap and therefore energy evanesces into the substrate. By removing a single metallic rod of the periodic lattice, a defect resonator can be created. This

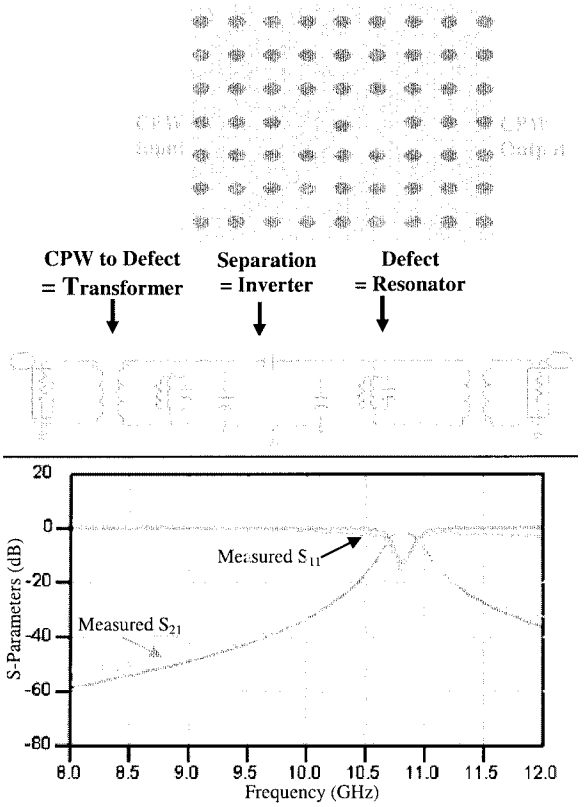

Fig. 3. Two-pole filter made from defects in a periodic metal lattice. (a) Schematic of the filter. (b) Equivalent circuit. (c) Equivalent circuit results versus measured S-parameters.

defect resonator gives rise to a mode that resonates at the defect frequency within the bandgap. By creating multiple, coupled defect resonators, a filter can be created, as shown in Fig. 3.

A schematic of the metallodielectric filter is shown in Fig. 3. In short, the metallodielectric filter utilizes the fact that the field within a defect resonator is not strictly located internal to the resonator. The fields are loosely bound to the defect region. Therefore, by placing two resonators adjacent to each other, the resonator modes couple. By appropriately coupling in to the periodic lattice, critical coupling can be achieved and a bandpass filter created. In this case, shorting a coplanar waveguide (CPW) line that is printed between the inclusions provides the coupling to the defect (see Fig. 3). The H-field circulating the center signal path of the CPW line couples to the H-field with the same polarization within the defect region. A full discussion of the filter design is described in [11], which utilized a hand-milled large-scale model made of low dielectric constant Duroid 5880.

The effect of using alumina in the filter relative to Duroid is shown in Table I. For the equivalent implementation as in [10] (i.e., same height and transverse parameters adjusted to maintain the same frequency), the theoretical unloaded Q of a single resonator is increased from 761 to 1250. Each of the loss mechanisms listed in the table add in parallel. As seen in the table, in the Duroid structure, the dielectric loss is the limiting factor, but for the implementation in alumina, the dielectric loss is nearly negligible. The effect of the dielectric loss is mitigated by an order of magnitude as the dielectric Q is increased from 1110 to

TABLE I
COMPARISON OF A DUROID AND ALUMINA METALLODIELECTRIC RESONATOR

3 mm Metallo-Diel. Resonator	Duroid (ε_r=2.2)	Alumina (ε_r=9.8)
$Q_{UNLOADED}$	**761**	**1250**
$Q_{DIELECTRIC}$	1,110	10000
Q_{METAL}	2,200	1500
$Q_{LEAKAGE}$	>10,000	>10,000

$\sim$ 10 000. In addition, the structure is reduced in size by more than a half due to the increase in dielectric constant.

For the example constructed in this study, the measured results of the metallodielectric filter are shown in Fig. 3(c). The filter designed in alumina has metallic inclusions with a diameter of 1.8 mm. The inclusions are placed in a rectangular lattice spaced 4 mm apart transversely and 3.1 mm longitudinally along the filter. The spacings of the posts defining the resonators were adjusted to provide a $-$3-dB bandwidth of 2.1%. The EBG substrate filter was made relatively thin, 700 μm, which shows the capabilities of the fabrication for thin substrates, but also limits the theoretical unloaded Q to a value of 645. Even without deembedding the loss of the CPW lines feeding the filter, the insertion loss of the filter is just $-$1.15 dB. In Section IV-A, these results are used to extract the dielectric loss of the finished structure.

A. Loss Characterization of Material After Processing

Alumina is theoretically a low-loss ceramic. However, if the material has imperfections due to the fabrication process, additional loss is added. The material in its finished form after all processes including metallization must be characterized. There are many loss mechanisms that could compromise the performance of the ceramic structures. One of these mechanisms is the density of the ceramics. Dense ceramics are known to have much better loss parameters [14]. In addition, deformations such as miniature cracks that may be formed during fabrication may cause loss in the metal when it is plated or evaporated onto the substrate. Therefore, a means of determining the loss of the material in the exact, postfabricated state is desired. To get an accurate portrayal of the loss parameters, an equivalent circuit of the filter was constructed. Matching the performance of the equivalent circuit and the realized filter allows a comparison between expected and measured resonator Q's of the filter. Therefore, the dielectric performance can be determined.

Though simple formulas relating the insertion loss and bandwidth to the individual Q's of the resonator are given in many filter books, for example, [15], these general formulas use crude approximations and are not based on the specific filter (passband ripple and transfer function) designed. For a more accurate characterization, an equivalent circuit of the filter elements was developed to accurately describe the parameters of the filter. Through these means, specific loss values can be assumed and adjusted to match the actual measurements. When the bandwidth and insertion loss match with the measured data, then the resonator equivalent circuit has the correct assumed losses. Therefore, the unloaded Q of the individual resonators of the fabricated filter can be obtained. In turn, the losses assumed by the equivalent circuit can then be compared to the losses calculated via an eigenvalue analysis of a single resonator. The value of the loss inherent to the substrate in the eigenvalue simulation was optimized until the Q of the simulation matched that found through the equivalent circuit. By this method, the physical measurement of the filter (i.e., insertion losses and bandwidth) can be directly related to the value of the loss tangent of the material.

The equivalent circuit, shown in Fig. 3(b), approximated the coupled defects as parallel resonators connected by J-inverters. The J-inverters, modeled in the circuit by a junction of capacitors, are physically controlled by the lattice period in the vertical dimension [with reference to Fig. 3(a)] along with the diameter of the rods. The smaller the rods (or the further that they are spaced apart), the greater the coupling between resonators and the greater the value of the coupling coefficient characterized by the J-inverter. By adjusting the loss in the resonator, the equivalent circuit indicates that the resulting bandwidth to insertion loss pair (2.1% $-$3-dB bandwidth and $-$1.15-dB insertion loss) corresponds to a measured unloaded Q of 643. The correspondence of the equivalent circuit and the measured results are shown in Fig. 3(c).

To determine the properties of the resonator itself, namely to separate out the dielectric loss from the metallic loss, an eigenvalue solution of a single resonator was performed. The following relation relates the Q_{UNLOADED} to the metal and the dielectric losses:

$$\frac{1}{Q_{\mathrm{UNLOADED}}} = \frac{1}{Q_{\mathrm{METAL}}} + \frac{1}{Q_{\mathrm{DIELECTRIC}}}. \qquad (1)$$

There is also a third term, Q_{LEAKAGE}, which represents the amount of energy that leaks through the periodic substrate surrounding the defect region. This term is not shown in equation because it is negligible for metallodielectric substrates with more than two periods surrounding the defect. To provide the Q_{METAL}, a single resonator was simulated using the Ansoft HFSS program. Using only metallic loss in the eigenvalue solution, the Q_{METAL} was determined to be 691. Using (1) in conjunction with the measured value of Q unloaded and the derived value of the metal Q, the $Q_{\mathrm{DIELECTRIC}}$ is in the range of 9523 corresponding to a loss tangent of $\sim$ 1.05 e-4. This value is what is expected for dense, high-quality alumina at this frequency range. This study shows that the processing does not introduce impurities or major cracks into the structure that would increase the loss. As a result, this process is deemed to be a good method to make low-loss structures even with all of the manipulation of the ceramics.

V. ALL-DIELECTRIC 2-D RESONATOR

A more advanced design that presented a fabrication challenge is the all-dielectric 2-D EBG substrate as shown in Fig. 4. This resonator consists of a fully periodic row of dielectric rods with planar support layers on either side to create a parallel plate. The rods are spaced to inhibit propagation in two dimensions. Therefore, if rods are removed from the periodic array within the substrate, energy is localized within the aperiodic section and a defect mode is created. Since the energy is bound

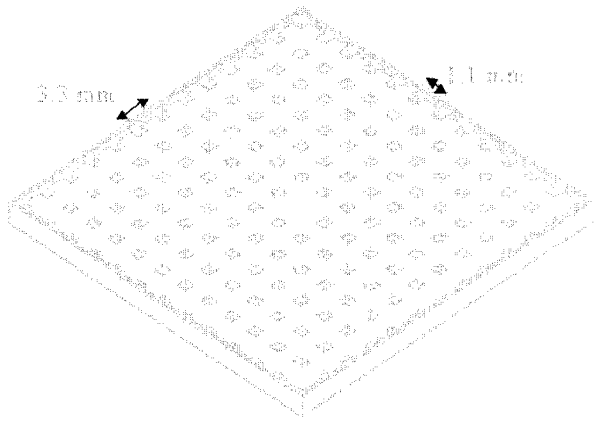

Fig. 4. Schematic showing a 2-D periodic substrate. The defect region, the removed rod in the center of the substrate, creates field localization and a resonance. There is a thin layer of alumina on the top and bottom for support of the rods.

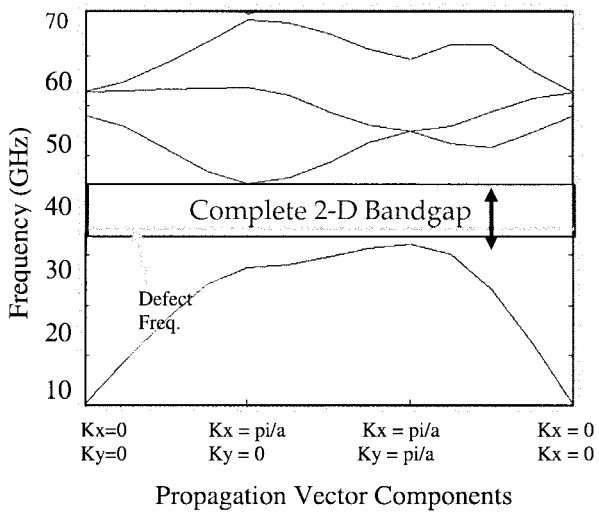

Fig. 5. Dispersion diagram of a 2-D periodic square lattice substrate. The bandgap is the region where the periodic wave function does not have real eigenvalues. Within the gap, a defect state is created by disrupting the lattice periodicity.

by dielectric sidewalls, the Q can be relatively high. This component cannot be fabricated as a single piece of low-loss ceramic in any other fabrication method known to the authors. In contrast, piece-by-piece fabrication is slow and repeatability is questionable.

The periodic substrate itself was analyzed using a plane wave expansion in two dimensions. A ratio of rod diameter to period of 1/3 in a square lattice gives a bandgap as shown in the dispersion diagram in Fig. 5. To determine the dispersion diagram, the wave equation manipulated for periodic materials is solved for eigenfrequencies for each propagation vector on the edge of the Brillouin diagram. The frequency region in which no real eigenvalues are found on the Brillouin zone is termed the bandgap. For the simple square lattice used in this example, the Brillouin zone is a triangle of propagation vectors ranging from $\mathrm{kx} = 0$ to pi/a, then extending from $\mathrm{ky} = 0$ to pi/a, then back to $\mathrm{kx} = \mathrm{ky} = 0$, where a is the period of the lattice. For each of these pairs of components of the propagation vector on the edge of the Brillouin zone, the eigenvalues (corresponding to a propagating frequency) are determined. A detailed example of this type of calculation is given by Smith [16]. For the range of frequencies where no real eigenvalues exist, the substrate does not propagate energy in the lowest order parallel-plate mode. After the determination of this range of frequencies, the removal of a single rod in the square lattice results in a defect resonant state. The defect frequency resonance is created by the multiple reflections from the surrounding EBG substrate which blocks energy propagation. The defect frequency is shown as an allowed state within this bandgap region in which frequencies are not allowed to propagate.

In the past [10], the resonators were demonstrated in bulky, hand-milled Duroid versions, which were limited in accuracy. These limitations came from the milling and the ability to bond the parallel plates from multiple stacked substrates. The resonator has been shown to give a relatively high Q for a planar structure. The design is similar to that shown previously in that it is created by the removal of a single rod, but there are major design concerns when scaling to higher frequencies in a ceramic material. The height of the structure itself as well as the height of the supporting rods becomes electrically thick. In the low-frequency design, these two factors can be addressed with only a slight perturbation of the original design.

The finished structure consists of two thin parallel alumina plates separated by an array of periodic alumina posts, as shown in Fig. 1. A strictly 2-D mold, such as that shown in Fig. 4, is modified by the addition of an upper and lower cavity with a raised boundary that will define the border of the substrate and thickness of the two support plates. For ideal bandgap performance, the plates should be kept as thin as possible. The 2-D plane-wave expansion from which the substrate was designed assumes that the periodic rods are sandwiched in a parallel plate without supports. The supports are added as a slight perturbation of this original design. In fact, it is the thickness of these plates that limit performance and to the frequency in which these parts can be scaled. The smallest thickness of the plates formed in the casting process is limited by the z-axis resolution of the build tool used to make the mold. For the 3-D inkjet printer, each of the layers is 50.8-μm thick. To ensure continuity of the plates, and the stability of the structure, the molds are made such that the plates are 250-μm thick after casting and ground to an acceptable thickness using diamond-grinding wheels. The support plates are coated with metal to form the parallel plate mode, which is interrupted by the periodic inclusions. The rods in the example shown above in Figs. 4–6 are 1.1 mm in width in a square lattice with period of 3.3 mm. The height of the rods and thus the inner spacing of the dielectric support layers is 1 mm.

Theoretically, the achievable unloaded Q for a 1-mm-high resonator (without support plates) at 32 GHz is 2021. However, this factor is compromised by the introduction of the thin plates used for support. The Q is derived by the formula

$$\frac{1}{Q_{\mathrm{UNLOADED}}} = \frac{1}{Q_{\mathrm{METAL}}} + \frac{1}{Q_{\mathrm{DIELECTRIC}}} + \frac{1}{Q_{\mathrm{LEAKAGE}}} \tag{2}$$

where Q_{METAL} is attributed to the conductor loss, $Q_{\mathrm{DIELECTRIC}}$ is the inverse of the loss tangent multiplied

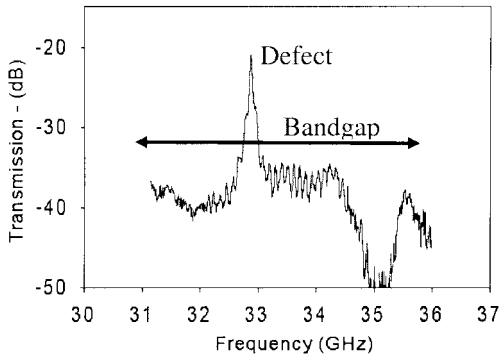

Fig. 6. Measured transmission between two slots in the substrate with a defect resonator within the bandgap.

times the amount of energy in the dielectric, and Q_{LEAKAGE} is due to the amount of energy leaking through the lattice surrounding the defect. For a thin, planar implementation, the major loss factor in the resonator is the metallic loss of the parallel plate. This is quantified by the formula

$$Q_{PP\_\mathrm{METAL}} = \frac{\omega \mu h}{2R} \tag{3}$$

where ω is the angular frequency, μ is the permeability, h is the height, and R is the surface resistance. The parallel-plate metal loss is much greater than the dielectric loss and the radiative loss. In an alumina resonator, the dielectric loss is nearly negligible. In addition, due to the number of period surrounding the defect (four layers), the leakage through the substrate is negligible as well. Quantitatively, both of these Q factors are greater than 10 000 [10]. Analyzing (3) reveals that the resonator Q increases linearly with height when the dielectric and leakage losses are negligible, therefore thicker substrates produce larger values of unloaded Q.

The results of the fabricated resonator are shown in Fig. 6. This plot is the transmission response through the substrate. The substrate is coupled through a transition from an external waveguide to a slot in the parallel plate. The slots are oriented such that their length is perpendicular to the defect. In this manner the H-field of the slot is parallel to the H-field in the resonant mode and coupling to the resonator occurs. The resonance within the bandgap is shown as a spike in transmission of -22 dB at the defect frequency. Away from resonance, coupling is limited between the slots by the periodic rods and is approximately -40 dB in the bandgap. The design was intentionally weakly coupled in order to extract the unloaded Q of the resonance. An analysis of the width of the transmission spike reveals an unloaded Q of 928. The Q is less than the theoretical value of the defect mode without supporting plates, but this is due to the perturbation of the thin support layers. The thin support layers (for clarity see the top right of Fig. 1) have two effects on the resonator. The layers increase the amount of energy that is in the dielectric, which in turn increases the dielectric loss and lowers the resonant frequency. Also, the support layers decrease the amount of attenuation per period, which increases the amount of energy leaking through the substrate away from the resonator. The optimization of the resonator and the analysis of the supports on the loss mechanisms will be the subject of future work.

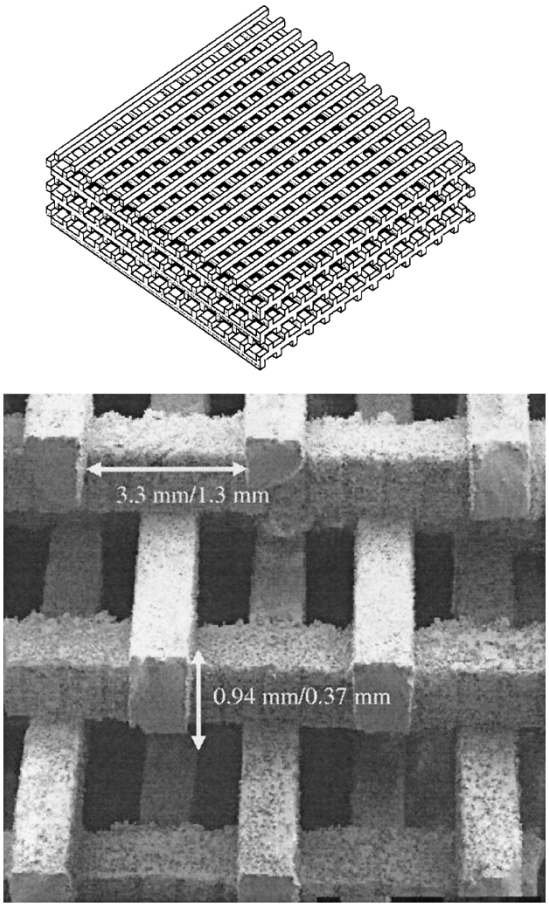

Fig. 7. CAD file and SEM of woodpile material including sizes for different frequency ranges. Dimensions indicate the two size scales that were fabricated.

VI. 3-D Woodpile EBG Structures

An even more fabricationally difficult challenge is presented by the formation of fully 3-D materials. To demonstrate the abilities of this technique, periodic "woodpile" dielectric structures were created (Fig. 7). At high frequencies $(>30$ GHz$)$, the structures have relatively minute inclusions. To test the novelty of this process, the structure was shifted to frequencies higher than that previously achievable in low-loss substrates [18]. The woodpile had previously been attempted at X-band through manual stacking of alumina rods. Though useful for a proof of concept, this fabrication results in a part that is nearly the size of a shoebox, which is impractical in most applications. In addition, similar structures at a smaller scale have been attempted in silicon by micromachining. Though effective to make precise features at much higher frequencies, even up to optical ranges [13], polysilicon has a loss that is an order of magnitude higher than that of alumina (loss $\tan \sim 0.02$ to 0.002 for silicon relative to 0.0001 for alumina). Since many of the proposed applications, such as low-loss reflective surfaces and defect resonators depend on a low-loss material [17], the low loss that only materials such as ceramics can provide is crucial.

To prove the variety of capabilities of the process, two frequency ranges were chosen, a 35–55-GHz version and an 88–120-GHz version. Due to the size of the structure, the 35-GHz version was developed with 12 criss-crossed

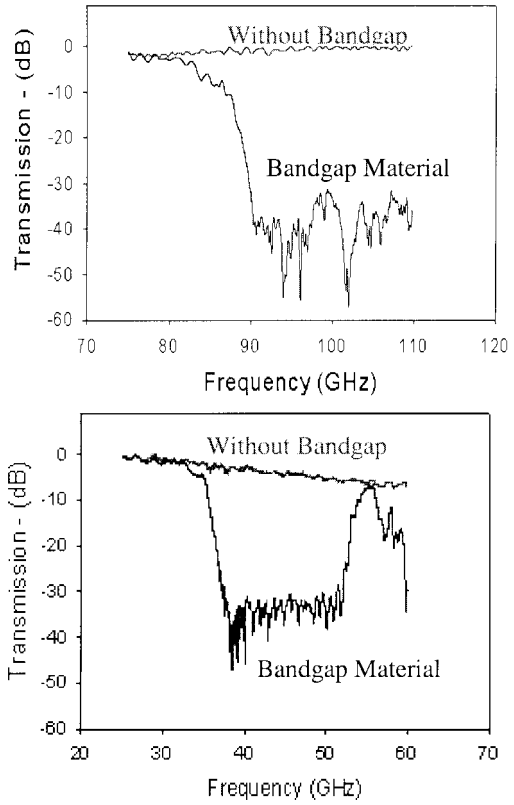

Fig. 8. Transmission through the stacking direction of scaled woodpile materials. (*top*): 0.37 mm rods: 14 layers. (*bottom*): 0.94 mm rods: 12 layers.

layers (three full periods), while the smaller W-band bandgap was developed with 14 layers (four full periods). The lower frequency region shows that the process can make relatively larger structures ($\sim$60 mm across in total with 0.94-mm rods inclusions spaced 3.3 mm apart). The smaller, high-frequency version shows the precise, minute features capable from this process (rods $\sim$0.37 mm with a spacing of 1.3 mm).

The structure was measured by analyzing the propagation through the material when it was placed in between two horn antennas. The setup used an absorber external to the material to block undesired radiation from corrupting the isolation. The frequency response was then measured with an HP 8510 network analyzer. The results are shown in Fig. 8. The null can be seen to be on average 35 dB deep for the lower frequency structure and lower than 42 dB for the higher frequency structure. The jitter in the bandgap can be interpreted as noise due to the finite size of the material and from multiple reflections from the test setup. The frequency range is similar to those found in [18] when their larger object's response is scaled to the correct frequency range.

A detailed analysis of the resulting postprocessed structure can be compared to the desired CAD file. A dimensional analysis was done through the use of National Institutes of Health (NIH) Image spatial analysis software.[1] In short, the analysis compares the desired CAD file to a high-resolution photograph of the fabricated structure. The average positional error of the relative spacing of the rods is 0.93%. This is a measure of the desired distance between the centers of each of the rods. In addition a measure of the desired area of each of the rods in a cross section of the structure was performed. This comparison of the total area of the rods gave an average error of 1.7%. For high-frequency operations, as previously stated, the dimensions must be precise, so the tolerances are a limiting factor in the utility of this process. For the proposed resonant applications, such as high-Q defect mode resonators, this tolerance is the single most important factor in making a relevant product. Variances are a factor of the shrinking variance due to the alumina solids loading in the slurry mixture, slight warping due to internal stresses for the burn out and sintering cycles, and the alignment of the 3-D printer in the mold making.

[1]Public domain NIH Image software program developed at the U.S. NIH.

A. Effective Medium Characterization

It is desirable to have a simple analytic expression for the complex structure in order to quickly analyze and understand the structure. The formal and most popular way of characterizing a 3-D woodpile is to perform a plane wave expansion in three dimensions and determine the full dispersion diagram. This method, though an effective analysis tool, is reasonably complicated and the physical mechanisms for the attenuation of the field are lost in the process. It is limited in its ability to facilitate the design of new structures. Therefore, to get an accurate determination of the propagation through the 3-D woodpile, an effective medium approximation was utilized. Since the measurement setup tests the propagation in specified directions, the 3-D structure can be modeled as a series of effective dielectric slabs in a series [19]. For propagation in a single direction (a slice on the 3-D dispersion diagram), which is the easiest measurement to verify the operation of the material, an effective medium approximation is applicable. Through this method, simple design rules and characteristics can be determined.

For example, to view the woodpile structure for transmission through the stacking axis of the woodpile, the structure is a series of TE and TM rods in rectangular lattices. TE is in reference to the polarization in which the electric field is perpendicular to the length of the rods. TM is the condition where the electric field is perpendicular to the length of the rods. As shown by Rytov [20], rods in this simple arrangement have effective dielectric constants

$$\varepsilon_{\text{eff}}\text{TE} = \varepsilon_o + \frac{\pi^2}{3}\left[f(1-f)(\varepsilon_2-\varepsilon_1)\right]^2\left(\frac{P}{\lambda}\right)^2 + O\left(\left(\frac{P}{\lambda}\right)^4\right) \tag{4}$$

$$\varepsilon_{\text{eff}}\text{TM} = \frac{1}{a_o} + \frac{\pi^2}{3}\left[f(1-f)\frac{(\varepsilon_2-\varepsilon_1)}{\varepsilon_2\varepsilon_1}\right]^2 \times \frac{\varepsilon_o}{a_o^3}\left(\frac{P}{\lambda}\right)^2 + O\left(\left(\frac{P}{\lambda}\right)^4\right) \tag{5}$$

where f is the filling fraction of the periodic material with dielectric constant ε_2 embedded in ε_1 with a transverse period P, ε_o is the volumetric average of the dielectric in the layer, while a_o is the volumetric average of the inverse, given by $f/\varepsilon_2+(1-f)/\varepsilon_1$. By approximating the 3-D object as a one-dimensional (1-D) stack, the analysis is simplified and the physical factors determining the bandgap frequency range are easily distinguishable. This gives a simple means of analyzing the structure and

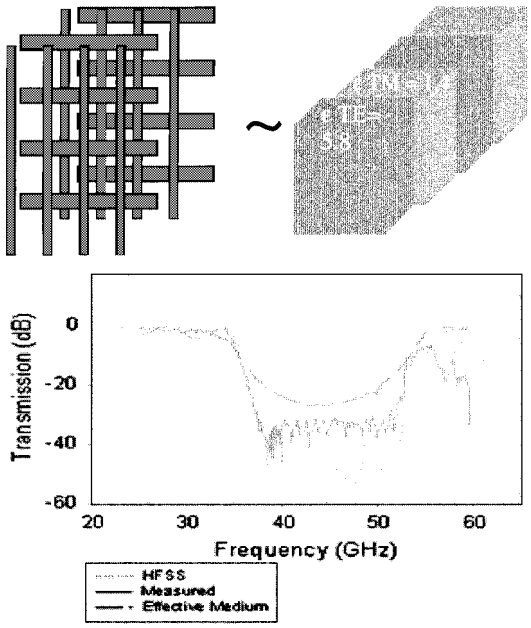

Fig. 9. Approximation applied to propagation through the Gamma-X crystal direction of the lattice.

evaluating the performance of the woodpile after it is built and measured.

The approximation gives guidelines for how to design the bandgap structures and indicates how to create larger reflections in given directions if desired. The maximum reflection for a given contrast in dielectric constant comes from dimensions which result in an effective 1-D quarter-wave stack, i.e., if the spacing was designed so that each layer had a thickness in the specified direction

$$t = \frac{\lambda_o}{4\sqrt{\varepsilon_{\text{eff}}}}.$$

As a result, not only is the ratio of the constants of the effective dielectric important, but the resulting effective electrical length of each layer is significant as well.

The results from the effective medium analysis are shown in Fig. 9. The effective medium approximation gives the effective dielectric constant through the layers to be 5.8 and 1.4 through the TE and TM layers, at the center of the bandgap. These effective layers when stacked together with the same length as the lower frequency woodpile provide a bandgap which stretches from 35 to 56 GHz. These cutoff frequencies for the bandgap in this direction can be seen to match up well. The approximation leaves the depth of the null significantly less than the measured result indicating that there are interactions of the 2-D rods beyond what the approximation accounts for. However, the location of the bandgap is correctly predicted and therefore this is deemed a useful tool for designing the bandgap with simple design criteria. In addition, in Fig. 9, the response from a full-wave simulation performed with Ansoft HFSS is provided. This simulation mimics the response of an infinite structure. The boundary conditions applied enforce a slight approximation that the tangential electric fields vanish at the top of each period. Therefore, the differences in the general shape and depth of the null in the bandgap can be attributed to both approximation and the finite size of the sample measured. However, the range of frequencies for the bandgap is accurately predicted with the approximate method and this should lead to new designs in future work.

VII. Conclusion

In this paper, the process of SFF fabrication applied to high-frequency periodic structures was discussed. The creation of low-loss materials incorporating macroscopic inclusions was attempted and verified. The manipulation of low-loss materials opens the possibility of many new structures that traditional flat, homogeneous substrates cannot create. Three specific applications to periodic structures were analyzed and the performance of the materials was critiqued. In summary, a relatively simple two-pole metallodielectric filter was developed to determine and demonstrate the low-loss characteristics of the material after full processing. The material after processing was shown to have a loss tangent approximately 1.05 e-4, which in turn results in a $Q_{\text{DIELECTRIC}}$ of approximately 10 000. In addition, to show the advanced processing capabilities, more fabricationally difficult periodic structures were analyzed, specifically the 2-D and 3-D EBG materials. These structures could not be easily fabricated out of low-loss materials through any other method known to the authors. A critical dimensional analysis was performed on the most advanced structure, the 3-D woodpile structure. The results indicate that less than 2% of error was incurred by the full processing, including molding, heating, and shrinking by volume and area. These results indicate that this method can be utilized as a reliable fabrication method for other original periodic 3-D structures utilized at high frequencies. In addition, however, the process technique is general enough to be utilized for many other types of applications as well.

References

[1] L. Brillouin, *Wave Propagation in Periodic Structures*. New York: Dover, 1946.

[2] S. T. Peng, T. Tamir, and H. L. Bertoni, "Theory of periodic dieelctric waveguides," *IEEE Trans. Microwave Theory Tech.*, vol. MTT-23, pp. 123–133, Jan. 1975.

[3] *J. Opt. Soc. Amer. B (Special Issue)*, vol. 10, Feb. 1993.

[4] T. M. Chu, "Solid freeform fabrication of biomaterials," Ph.D. dissertation, Univ. Michigan at Ann Arbor, Ann Arbor, MI, 1999.

[5] C. J. Reilly, "Novel electroactive ceramic architectures by indirect solid freeform fabrication," Ph.D. dissertation, Univ. Michigan at Ann Arbor, Ann Arbor, MI, 2001.

[6] S. Kang, A. G. Cooper, J. Stampfl, F. Prinz, J. Lombardi, L. Weiss, and J. Sherbeck, "Fabrication of high quality ceramic parts using mold SDM," in *Proc. Solid Freeform Fabrication Symp.*, Austin, TX, Aug. 1999, pp. 427–434.

[7] K. Venkataswamy, R. Waack, B. E. Novich, and J. W. Halloran, "Forming whisker reinforced sintered ceramics with polymerizable binder precursors," U.S. Patent 4 978 643, 1990.

[8] J. J. Beaman, J. W. Barlow, D. L. Bourell, R. H. Crawford, H. L. Marcus, and K. P. McAlea, *Solid Freeform Fabrication: A New Direction in Manufacturing*. Norwell, MA: Kluwer, 1997.

[9] Shumpert, Chappell, and Katehi, "Parallel-plate mode reductioin in conductor-backed slots using electromagnetic bandgap substrates," *IEEE Trans. Microwave Theory Tech.*, vol. 47, pp. 2099–2104, Nov. 1999.

[10] W. J. Chappell, M. P. Little, and L. P. B. Katehi, "High Q two dimensional defect resonators—Measured and simulated," in *IEEE MTT-S Int. Microwave Symp. Dig.*, vol. 3, 2000, pp. 1437–1440.

[11] ——, "High isolation planar filters using EBG substrates," *IEEE Microwave Wireless Comp. Lett.*, vol. 11, pp. 246–248, June 2001.

[12] E. Ozbay, A. Abeyta, G. Tuttle, M. Tringides, R. Biswas, T. Chan, C. M. Soukoulis, and K. M. Ho, "Measurement of a three-dimensional photonic band gap in a crystal structure made of dielectric rods," *Phys. Rev. B, Condens. Matter*, vol. 50, no. 3, pp. 1945–8, July 1994.
[13] S. Y. Lin and J. G. Fleming, "A three-dimensional optical photonic crystal," *J. Lightwave Technol.*, vol. 17, pp. 1944–1947, Nov. 1999.
[14] R. S. Jenson, "Ceramic substrate for hybrid applications," in *Hybrid Microelectronics Handbook*. New York: McGraw-Hill, 1995, ch. 2.
[15] G. L. Matthei, L. Young, and E. M. T. Jones, *Microwave Filters, Impedance Matching Networks, and Coupling Structures*. Norwood, MA: Artech House, 1980.
[16] R. D. Smith, "Analysis and experimental observations of two-dimensional photonic band gap structures," M.S. thesis, Univ. California, San Diego, CA, 1994.
[17] E. Ozbay, G. Tuttle, M. Sigalis, C. M. Soukoulis, and K. M. Ho, "Defect structures in layer by layer photonic band-gap crystal," *Phys. Rev. B, Condens. Matter*, vol. 51, no. 20, May 1995.
[18] ——, "Measurement of a three-dimensional photonic bandgap in a crystal structure made of dielectric rods," *Phys. Rev. B, Condens. Matter*, vol. 50, no. 3, July 1994.
[19] P. Lalanne, "Effective medium theory applied to photonic crystals composed of cubic or square cylinders," *Appl. Opt.*, vol. 35, no. 27, Sept. 1996.
[20] S. M. Rytov, "Electromagnetic properties of a finely stratified medium," *Sov. Phys. J.*, vol. 2, pp. 466–475, 1956.

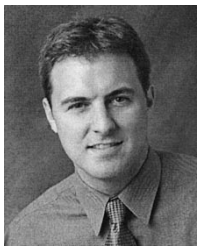

William J. Chappell received the B.S.E.E., M.S.E.E., and Ph.D. degrees from The University of Michigan at Ann Arbor, in 1998, 2000, and 2002, respectively.

His work focuses on periodic and composite materials for use in high-frequency circuits and antennas. He also works with silicon micromachining, polymer formation, and low-loss ceramics for the formation of these materials. In addition, his research interests include rapid prototyping, freeform fabrication, and small-scale formation of electrically functioning ceramic and polymer passive components. He recently joined the faculty at Purdue University, West Lafayette, IN, as an Assistant Professor. He is a member of the Birck Nanotechnology Center, the Center for Wireless Systems and Applications, and the Bill Elmore Microwave and RF Laboratory.

Chris Reilly received the B.S. degree in mechanical engineering from the Worcester Polytechnic Institute, Worcester, MA, and the M.S and Ph.D. degrees in materials science and engineering from The University of Michigan at Ann Arbor.

He currently leads the Engineering Department, Adaptive Materials Inc. (AMI), Ann Arbor, MI. His efforts within AMI's Defense Advanced Research Projects Agency (DARPA) project focus on SOFC electrode design and fuel cell testing. His eight years of industrial and academic ceramic processing experience are well suited to the task of refining AMI's proprietary manufacturing techniques. Prior to joining AMI, he was a Process Development Engineer for the Industrial Ceramics Branch of Saint Gobain and an engineering consultant to both the Silicon Carbide Division, Norton Company and Norton Céramiques Avancées du Canada.

John Halloran is the Department Chair and A. H. White Collegiate Professor with the Department of Materials Science and Engineering, The University of Michigan at Ann Arbor. He currently devotes 20% of his time to Adaptive Materials Inc. (AMI), Ann Arbor, MI. He has been very active in all aspects of ceramic processing and manufacturing for more than 30 years. Throughout his industrial and academic career, he has played a significant role in numerous emerging ceramic technologies. His experience includes fund raising and management for numerous research and development programs, several of which have been successfully transitioned into the commercial marketplace. Prior to becoming a Department Chair with The University of Michigan at Ann Arbor, he was the Vice President of Technology for CPS Inc., and a Professor at Case Western Reserve University.

Linda P. B. Katehi (S'81–M'84–SM'89–F'95) received the B.S.E.E. degree from the National Technical University of Athens, Athens, Greece, in 1977, and the M.S.E.E. and Ph.D. degrees from the University of California at Los Angeles, in 1981 and 1984, respectively.

In September 1984, she joined the faculty of the Electrical Engineering and Computer Science Department, The University of Michigan at Ann Arbor, as an Assistant Professor, and then became an Associate Professor in 1989 and Professor in 1994. She has served in many administrative positions, including Director of Graduate Programs, College of Engineering (1995–1996), Elected Member of the College Executive Committee (1996–1998), Associate Dean For Graduate Education (1998–1999), and Associate Dean for Academic Affairs (since September 1999). She is currently the Dean of the Schools of Engineering, Purdue University, West Lafayette, IN. She has authored or coauthored 410 papers published in refereed journals and symposia proceedings. She holds four U.S. patents. She has also generated 20 Ph.D. students.

Dr. Katehi is a member of the IEEE Antennas and Propagation Society (IEEE AP-S), the IEEE Microwave Theory and Techniques Society (IEEE MTT-S), Sigma Xi, Hybrid Microelectronics, and International Scientific Radio Union (URSI) Commission D. She was a member of the IEEE AP-S Administrative Committee (AdCom) (1992–1995). She was an associate editor for the IEEE TRANSACTIONS ON MICROWAVE THEORY AND TECHNIQUES and the IEEE TRANSACTIONS ON ANTENNAS AND PROPAGATION. She was the recipient of the 1984 IEEE AP-S W. P. King (Best Paper Award for a Young Engineer), the 1985 IEEE AP-S S. A. Schelkunoff Award (Best Paper Award), the 1987 National Science Foundation Presidential Young Investigator Award, the 1987 URSI Booker Award, the 1994 Humboldt Research Award, the 1994 University of Michigan Faculty Recognition Award, the 1996 IEEE MTT-S Microwave Prize, the 1997 International Microelectronics and Packaging Society (IMAPS) Best Paper Award, and the 2000 IEEE Third Millennium Medal.